ACS Catalysis

Review

pubs.acs.org/acscatalysis

Catalysts under Controlled Atmospheres in the Transmission Electron Microscope

Thomas W. Hansen* and Jakob B. Wagner

Center for Electron Nanoscopy, Technical University of Denmark, DK-2800 Kgs. Lyngby, Denmark

ABSTRACT: Over time, there has been an increasing interest in observing catalysts in their operating environment at high spatial resolution and ultimately to determine the structure of a catalytically active surface. One tool with the potential to do exactly this in direct space is the transmission electron microscope, and since its invention by Ernst Ruska, the idea of imaging samples under gaseous atmospheres was envisioned. However, microscopes have traditionally been operated in high vacuum due to sensitive electron sources, sample contamination, and electron scattering off gas molecules resulting in loss of resolution. Using suitably clean gases, modified pumping schemes, and short pathways through dense gas regions, these issues are now circumvented. Here we provide an account of best practice using environmental transmission electron microscopy on catalytic systems illustrated using select examples from the literature showing how in situ electron microscopy can provide new insight into the state of catalysts under reactive environments.

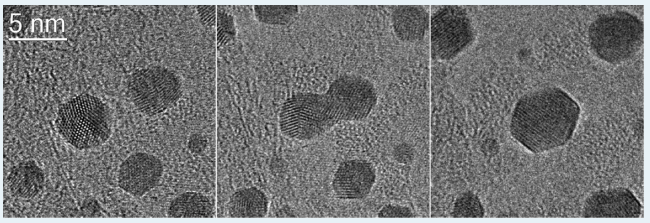

KEYWORDS: *TEM, in situ, controlled atmosphere, ETEM, EELS, EDX, catalysts*

INTRODUCTION

Chemical industry relies heavily on catalysts. Approximately 85−90% of all chemicals are made via catalytic processes.[1] Catalysts are used in processes ranging from synthesis of fine chemicals over fuel refinement to abatement of pollution. Heterogeneous catalysts are often composed of metal nanoparticles supported on a substrate providing a high dispersion and stabilization of the particles. The nanoparticle surfaces hold the active sites responsible for the conversion of reactants to products. As catalysts are dynamic entities, they restructure as a function of the reaction coordinate, and studies under a reactive environment are needed in order to unravel that function.[2] In situ electron microscopy can provide information on particle size distributions, the shape of catalytically active nanoparticles, and thereby the distribution of surface sites. Such knowledge combined with a quantum chemical treatment of the problem using density functional theory and microkinetical models enables prediction of the conversion of reactants to products and hence derivation of an overall reaction rate.[3,4] Addressing site-specific turnover numbers[5] remains a daunting challenge.

In order to obtain insight into the size, shape, and surface structure of catalytically active nanoparticles, a tool capable of obtaining overview information from larger areas as well as achieve atomic resolution of individual nanoparticles is required. Electron microscopy has the necessary resolution to fulfill these requirements and has had a large impact in heterogeneous catalysis science.[6−9] Electron microscopy provides direct imaging of structures, and contrary to techniques such as X-ray absorption near edge structural spectroscopy, spectroscopic information can be acquired with high spatial resolution within one instrument.[6] A direct measurement of not only particle size and shape but also particle/support interfaces and local chemical composition have provided scientists with valuable information about the success of their synthesis and catalyst evolution as a function of time on stream. Whereas catalysis scientists use a very wide range of characterization tools, some of these parameters are solely obtainable via electron microscopy. With the advent of aberration correction for transmission electron microscopy (TEM), catalysis researchers have gained a tool with the potential for unraveling the surface structure of catalytic materials with unprecedented resolution. With suitable peripheral equipment added to the microscope, it is possible to obtain information about composition and chemical state. Using these add-ons in combination with environmental capabilities provides researchers with the possibility to characterize the atomic structure of a catalyst in a reactive environment resembling the operating conditions of the catalyst. Combining local scale information gained from controlled atmosphere/environmental TEM (ETEM) with other complementary in situ techniques, it is possible to probe the working catalyst over length scales ranging from micro to nano.[10]

Despite the fact that catalysts often work at elevated temperatures and pressures, most TEM studies of catalysts are carried out at room temperature in high vacuum. Thus, often the results do not reflect the active state of the catalyst. Controlled atmosphere or ETEM provides a method for imaging samples under gaseous atmospheres at pressures of a few kPa at elevated temperature. The idea was already

Received: December 5, 2013
Revised: April 3, 2014
Published: April 4, 2014

conceived by Ruska, the inventor of the transmission electron microscope more than half a century ago.[11] The concept was further developed by Swann et al.,[12] Hashimoto et al.,[13] Baker et al.,[14] and into the differential pumping design often used today, by Gai et al.[15] The technique was extensively used in the 70s by Baker and co-workers to study mainly carbon filament formation[16] and particle mobility.[17]

Whereas heterogeneous catalysts can take many forms and shapes, this review will deal primarily with supported metal nanoparticles. Controlled atmosphere TEM is used extensively in other fields as well. Particularly in chemical vapor deposition,[18] selective oxidation catalysis,[19,20] carbon nanotube growth,[21−27] focused electron beam induced deposition,[28] and graphene manipulation.[29]

In this review, we have aimed at covering data from the period of the field-emission-based ETEM, starting from about the turn of the century. Older references have been included where appropriate. We have tried to focus on examples from the literature that illustrate and span the capabilities of ETEM in order to demonstrate how it can facilitate catalysis research. Environmental scanning transmission electron microscopy (ESTEM) is a closely related emerging technique, which has been deliberately left out of this review. ESTEM is described in a recent paper by Boyes et al.[30]

DESIGN, INSTRUMENTATION, AND PERFORMANCE

The main issues to address when introducing gas into the electron microscope is to confine the gas around the sample and maintain UHV conditions near the electron gun. Two routes have been pursued in order to fulfill these criteria: (1) The gas is confined near the sample by means of pressure-limiting apertures, and the vacuum in the remaining column is maintained by a differential pumping scheme. The pressure-limiting apertures are positioned in the objective lens in close proximity to the sample leaving a high-pressure zone less than 1 cm thick. The concept was described by Boyes and Gai[15] and further exploited on microscopes from various vendors.[31−35] A schematic drawing of the differential pumping approach is shown in Figure 1. This approach limits the obtainable pressure to ca. 10^3 Pa in the sample area. Within this scheme, two routes for gas inlet are used. These routes are either injection through the objective lens resulting in a uniform pressure between the pole pieces or direct injection onto the sample via a nozzle in close proximity to the sample providing a locally high pressure. (2) The gas is confined by solid electron transparent membranes allowing higher pressures in the vicinity of the sample without compromising the requirement of UHV near the electron gun. Placing two membranes, typically fabricated from silicon nitride or oxide, in a holder with a spacing of less than 100 μm, pressures exceeding atmospheric pressure can be obtained while preserving atomic resolution.[36,37]

Regardless of which route is chosen, gases have to admitted to the sample in a controlled manner, and a high degree of cleanliness must be observed. For this purpose, scientific-grade gases are typically used, and a cleaning system can be added to the inlet system in the form of vapor traps and filters in order to remove unwanted components. In order to keep a stable flow, high precision mass flow controllers are typically used.

One of the main concerns when admitting gas into the TEM is the effect it might have on microscope performance (i.e., resolution). As the electrons traverse the high-pressure gas zone, they are scattered by the gas molecules leading to a loss of

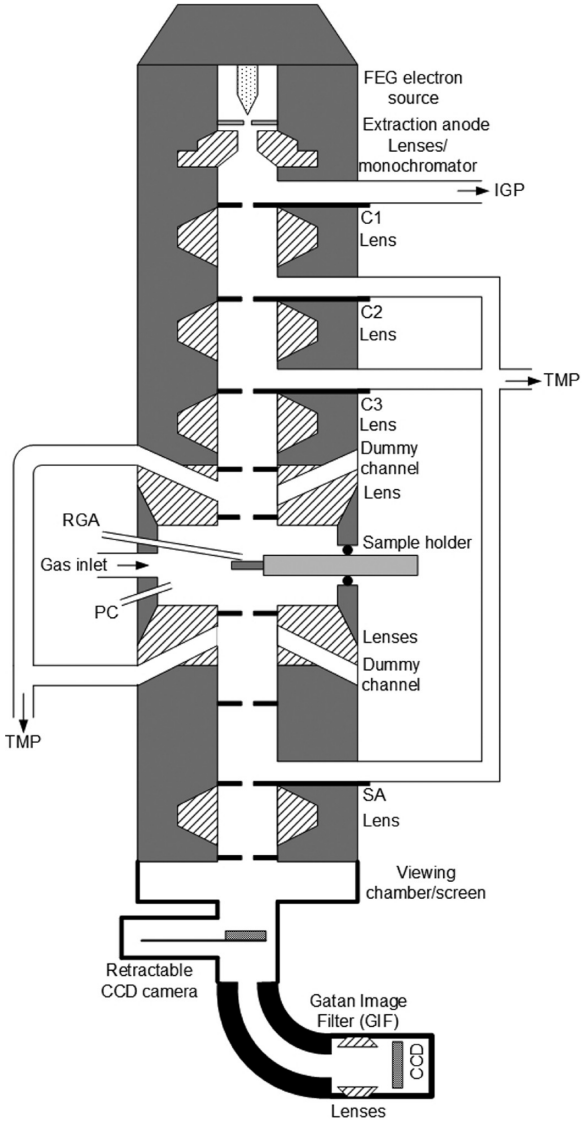

Figure 1. Sketch of differentially pumped ETEM.[31] The concept is based on the description of Boyes and Gai.[15] Reproduced with permission from ref 31. Copyright 2010 Maney Publishing.

intensity.[38−40] Larger gas molecules such as dinitrogen, dioxygen, and argon affect the electron beam intensity more than lighter molecules such as dihydrogen and helium. As the primary energy of the electrons is decreased, this becomes more severe due to the increased scattering cross section of the gas molecules. Furthermore, scattering is no longer confined to the sample plane, as the gas molecules will occupy a volume around the sample.[41] As the electrons interact with the gas molecules, the gas molecules may be ionized, resulting in a plasma in the high-pressure zone. This charged cloud of molecules can disturb the coherence of the electron wave, furthering the loss of resolution. This effect is illustrated in Figure 2 and was investigated in detail by Jinschek and Helveg.[42]

Imaging in the transmission electron microscope is hampered by the fact that electromagnetic lenses are far from perfect. Their performance has been compared to using the bottom of a glass bottle in an optical microscope. Recent developments have allowed manufacturers to correct for lens imperfections by the introduction of aberration correctors,[43] pushing the resolution limit beyond 1 Å,[44] allowing direct imaging and

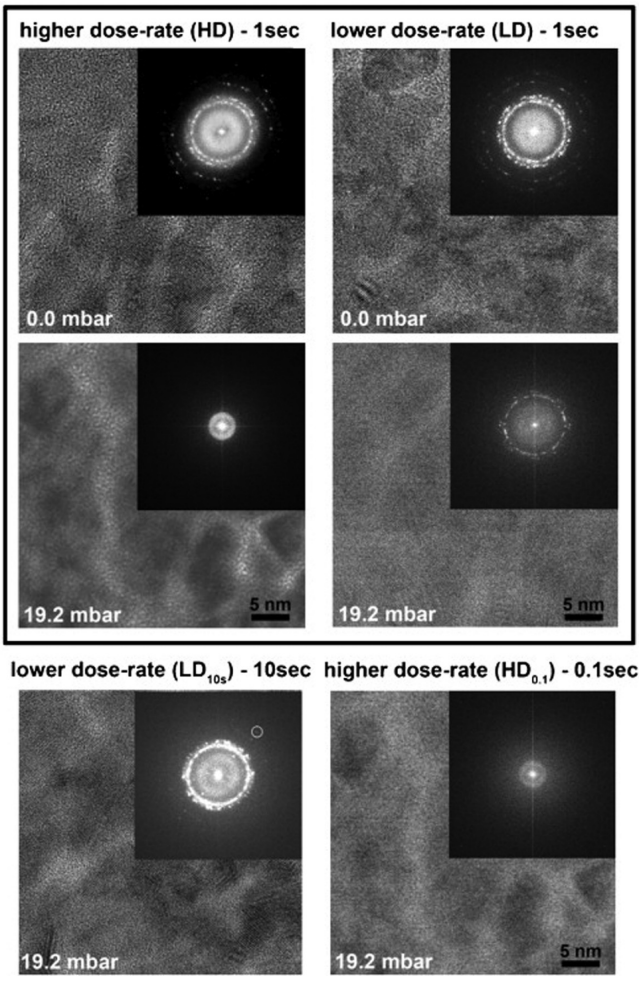

Figure 2. High-resolution images of an Au/C specimen with corresponding FFT displays inserted. The images were acquired under exposure to N_2 at electron beam dose rates of 10^5 e^-/nm^2 s (LD) and 10^6 e^-/nm^2 s (HD) respectively. Reproduced with permission from ref 42. Copyright 2012 Elsevier.

interpretation of atomic columns. Furthermore, the introduction of aberration correctors allow the pole piece gap to be expanded to 5 mm (maybe even 10 mm), maintaining high spatial resolution. This results in more freedom and space around the sample to introduce further equipment such as spectrometers and light sources.

Electron Beam Interaction with Gas Species. One of the biggest challenges of performing electron microscopy in a gaseous environment is the interaction of high-energy electrons with the gaseous species ionizing the molecules, which can influence the image formation. The latter will affect the contrast and spatial resolution. However, atomic resolution is still achievable on a routine basis using ETEM. More severe is the ionization of the gas molecules leading to chemically more active gas species near the sample. In general, the electron dose should be kept as small as possible when performing ETEM experiments without compromising the imaging quality. It is good practice to study the relation between electron dose and observed phenomena. Ideally, the observations should be compared to areas of the sample, which have not been exposed to the electron beam during gas exposure. Simonsen et al. conducted a thorough study in order to address the electron beam influence on Pt nanoparticles sintering in the ETEM under 1 kPa air.[45,46] This detailed study shows the importance of addressing the influence of the electron beam. Under high current density of the beam, shrinkage of the Pt nanoparticles was observed in the presence of oxygen in the microscope. This shrinkage was not observed in vacuum or in the presence of oxygen (without the electron beam) suggesting that the shrinkage is caused by removal of volatile Pt-oxygen species by the electron beam. Neglecting the importance of the potential effect of the electron beam might influence the deduced sintering mechanisms.

Another detailed study showing the importance of knowing the limitations of environmental TEM focuses on the Au/TiO_2 system for CO oxidation, where the $Au-TiO_2$ interface is strongly influenced by the surrounding gas in combination with an intense electron beam.[47] In the presence of oxygen and an intense electron beam, TiO_2 decorates and encapsulates the Au nanoparticles. Kuwauchi et al. showed that both the current density of the beam and the total dose of the high-energetic electrons have to be taken into consideration when designing the experiment.[47] Figure 3 summarizes the different effect the electron beam has on a Au/TiO_2 system.

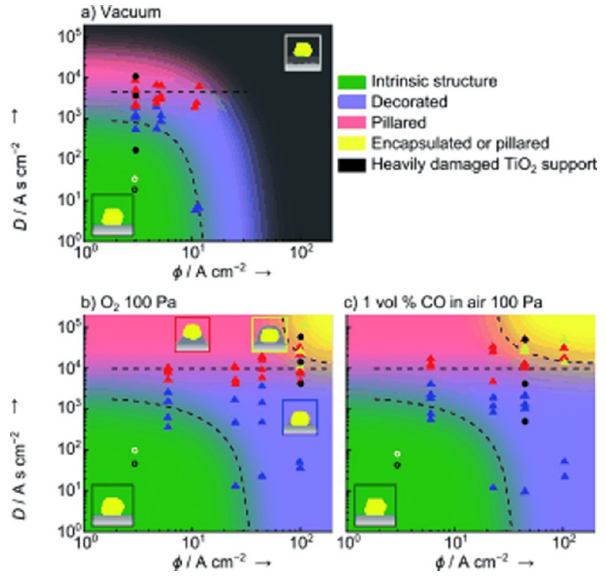

Figure 3. Structural changes of Au/TiO_2 catalyst under different gases varying the electron current density, φ, and the total dose, D, observed in ETEM. (a) Vacuum, (b) 100 Pa O_2, (c) 100 Pa CO/air (1:100). All observations at room temperature. Reproduced with permission from ref 47. Copyright 2012 Wiley.

Even the slightest amount of water in combination with a too intense electron beam can influence the behavior of some materials. Wagner et al. showed that 10^{-4} Pa of water causes severe alteration on MgO smoke cubes decorated with Au nanoparticles under electron beam exposure. In the presence of water and an electron beam, MgO nanopillars were grown under the Au nanoparticles.[41] With that in mind, residual gases from ETEM experiments can easily cause issues in successive experiments. In order to keep the environment in the ETEM as clean as possible, procedures on bake-out of the microscope and in situ plasma cleaning of the sample area should be routine in every ETEM laboratory.

The interaction of the high-energy electrons and the sample will to some extent give rise to an increased temperature of the probed sample area. Theoretical analysis by Gryaznov of the

dx.doi.org/10.1021/cs401148d | ACS Catal. 2014, 4, 1673−1685

heat flux has shown that the temperature of electron-irradiated nanoparticles might increase to several hundred degrees depending on contact conditions with the substrate, the intensity of the beam, and the size of the nanoparticles, with larger nanoparticles heating more in the electron beam.[48] However, in the work by Gryaznov, the interface area between particle and substrate is relatively small, and thereby the thermal conduction is limited. The electron-beam-induced heating of nanoparticles less than 10 nm is limited to a few degrees and should not be a significant issue unless the thermal contact between particle and support is extremely poor. In general, the local temperature in an in situ experiment depends on multiple parameters including several sources and sinks.

Experimental evidence of an electron-beam-induced increment of the local temperature was shown by Howe et al., in which they studied the melting behavior of submicrometer-sized Al−Si alloy particles supported on an amorphous carbon thin film using a relatively high electron beam current.[49] Doraiswamy and Marks showed that the electron-beam-induced heating is significantly lower for supported nanometer sized particles.[50] Again, the operator is encouraged to use as low a beam current as possible to avoid significant heating.

In a carefully planned experiment, the effects of the electron beam can be deconvoluted from the observed phenomena, thereby unleashing the full potential of ETEM experiments in fundamental studies of gas−solid interactions in catalyst systems.

APPLICATIONS WITHIN CATALYSIS

For supported catalysts, a parameter of interest is typically the particle size distribution. Unlike many other techniques such as X-ray diffraction, TEM can provide not only the mean particle size but also the size distribution. Admittedly, such a distribution will be obtained from only a limited subset of the particles, where XRD for instance can provide an estimate of the average size from a macroscopic amount of the sample. However, TEM can provide information far beyond the particle size distribution. In order to support the current trend in catalysis of engineering particles with a specific functionality, a technique capable of unravelling the atomic structure and behavior under reactive environments is needed.

However, knowing the particle size distribution and the surface structure under vacuum or inert conditions is typically not enough. As catalytic materials are exposed to various gas species at elevated temperatures, they tend to sinter, and their surfaces typically restructure. The restructured and often dynamic surface forms the basis for the "active" sites for a catalytic reaction. With the incorporation of aberration correctors on environmental transmission electron microscopes, a tool for resolving the surface structure of a metal nanoparticle under a gaseous atmosphere has become available.[38,51] Although morphology changes of the catalysts are observed under gaseous atmosphere in the ETEM, linking it directly to the activity of the catalyst is difficult as quantitative measurements of conversion and selectivity is far from an easy task in the ETEM setup. Efforts to measure conversion in situ in the ETEM will be discussed in a separate section in this review.

ON THE ACTIVE STATE OF SUPPORTED METAL CATALYSTS

Cu/ZnO − Methanol Synthesis. As the environment around metal nanoparticles changes, the fraction of different gases adsorbed on the surfaces changes. This can result in a change of the specific surface energy allowing for a restructuring of the particle. Using the first ETEM equipped with a field emission electron source, Hansen et al. demonstrated this effect on a Cu/ZnO methanol synthesis catalyst.[52]

As summarized in Figure 4, the catalyst was exposed to various environments found in the methanol synthesis reactor:

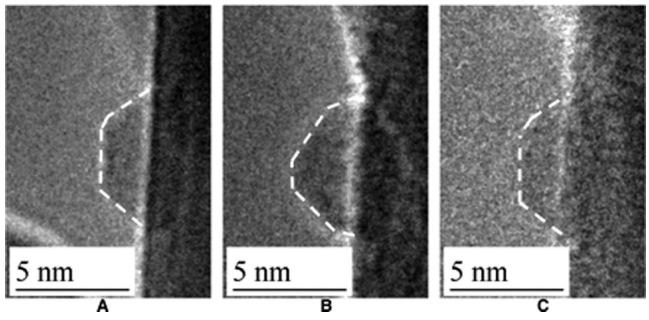

Figure 4. TEM images showing the reversible shape change of a Cu nanoparticle. The same Cu nanoparticle is imaged at 220 °C under (A) H_2 at 150 Pa, (B) H_2:H_2O (3:1) at a total pressure of 150 Pa, and (C) H_2 at 150 Pa. Reproduced with permission from ref 52. Copyright 2002 American Association for the Advancement of Science.

H_2, H_2/H_2O, and H_2/CO, all at 220 °C. In pure hydrogen, the copper particles appeared faceted exposing the low-index facets (100), (110), and (111). As the surroundings became more oxidizing by adding H_2O, the particles adopted a more spherical shape due to relative change in the facets' specific surface energies by adsorption of OH species. Under these conditions, the particles remained metallic, as determined by HRTEM analysis. When switching the environment to a more reducing environment by adding CO to the hydrogen, the particles again exposed facets; however, the distribution of the different facets changed, and the particles wetted the ZnO surface. Two explanations, which might both contribute to the observed effect, were suggested. First, the surface energy of the copper particles changes as CO adsorbs on the particle surface. Second, the surface of the zinc oxide support is slightly reduced, offering a different interface energy to the copper particle. In contradiction to the morphology changes observed as an effect of the H_2O treatment, the wetting of the Cu particles was observed to be irreversible when CO was removed after the CO/H_2 treatment, indicating that the major effect is caused by surface reduction of the ZnO. The chemical state of the Cu nanoparticles under the different environments was further studied by electron energy-loss spectroscopy. In all cases described above, Cu was found to be in the metallic state.[53] The findings from the ETEM studies were consistent with the results from Grunwaldt et al., who studied a similar catalyst system. Using EXAFS, it was determined that the morphology of Cu nanoparticles change reversibly during changes in the reaction conditions.[2] The study also confirmed that alloys of Zn and Cu do not form under methanol synthesis conditions. The metallic state of copper under reaction conditions was also confirmed in an infrared spectroscopy (FTIR) study by Topsøe

dx.doi.org/10.1021/cs401148d | ACS Catal. 2014, 4, 1673−1685

and Topsøe.[54] The morphology change of the Cu particles has been used as input for micro kinematical models in order to relate the distribution of facets to the activity.[54−56]

In a more recent study by Cabié et al.,[57] a similar phenomenon was observed for platinum nanoparticles. The platinum nanoparticles were mainly truncated by (001) facets in O_2 and mainly by (111) facets in H_2. Refaceting was again observed when the same set of nanoparticles were re-exposed to oxygen. The same group studied the refaceting further, including other catalyst systems as well.[58,59]

Au/Oxides − CO Oxidation. Typically, the outermost layers of a nanoparticle will restructure depending on the composition of the surrounding gas atmosphere. Observing the atomic configuration under a reactive environment is necessary in order to unravel the nature of the active site for a given reaction.

Despite gold being chemically inert in the bulk,[60] gold nanoparticles below about 10 nm are highly active for the oxidation of carbon monoxide to carbon dioxide even at temperatures below room temperature.[61,62] Gold nanoparticles have been studied extensively using electron microscopy, focusing specifically on nanoparticle sizes, surface structure, support interface, and growth.[63] For gold, nanoparticle growth is particularly important, as all activity is lost when the nanoparticles exceed a certain size.[64]

Using an aberration-corrected ETEM, Yoshida et al. investigated gold nanoparticles supported on cerium dioxide.[51] The catalyst was first observed in vacuum where the surface did not restructure as viewed in the ⟨110⟩ zone axis—see Figure 5.

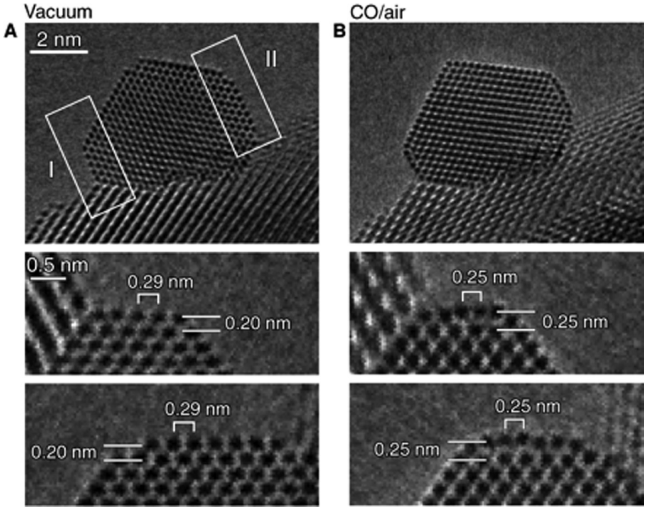

Figure 5. Au{100} reconstructed surface under catalytic conditions. The CeO_2 supported gold nanoparticle in (a) vacuum and (b) a reaction environment (1 vol % CO in air/gas mixture at 45 Pa at room temperature). Reproduced with permission from ref 51. Copyright 2012 American Association for the Advancement of Science.

As the sample was exposed to a mixture of 1% CO in air, the outermost gold layer expanded from 0.20 nm (as also observed in bulk Au) to 0.25 nm. The combination of the ETEM observations with ab initio calculations using the VASP package[65] show that the restructured gold nanoparticle surface accommodates a higher surface coverage of CO molecules compared to the bulk terminated structure due to an unusual bonding arrangement with the second gold layer. Similarly, Uchiyama et al. studied the shape of gold nanoparticles supported on cerium oxide in different atmospheres. Their main observation was that when exposed to CO/air mixtures, the gold nanoparticles were truncated by low energy {111} and {100} facets.[66]

Ru/BN − Ammonia Synthesis. Supported ruthenium nanoparticles have been found to be a highly active catalyst for ammonia synthesis.[67] Studies of Ru nanoparticles supported on carbon, boron nitride, magnesium aluminum spinel, and alumina have shown these catalysts to be significantly more active than traditional iron-based catalysts.[68−70] The addition of barium as promoter increased the integral reaction by more than a factor of 10. Hence, obtaining insight into the role of the promoter phase could provide valuable insight into the workings of this catalyst system.

When imaged in high vacuum at room temperature, the surface of the ruthenium nanoparticles was covered by a layered structure identified as hexagonal boron nitride, a strong indication of strong metal support interactions (SMSI).[71,72] This layer entirely disguised the surface structure of the metal nanoparticles (see Figure 6A,B). When exposed to a reactive

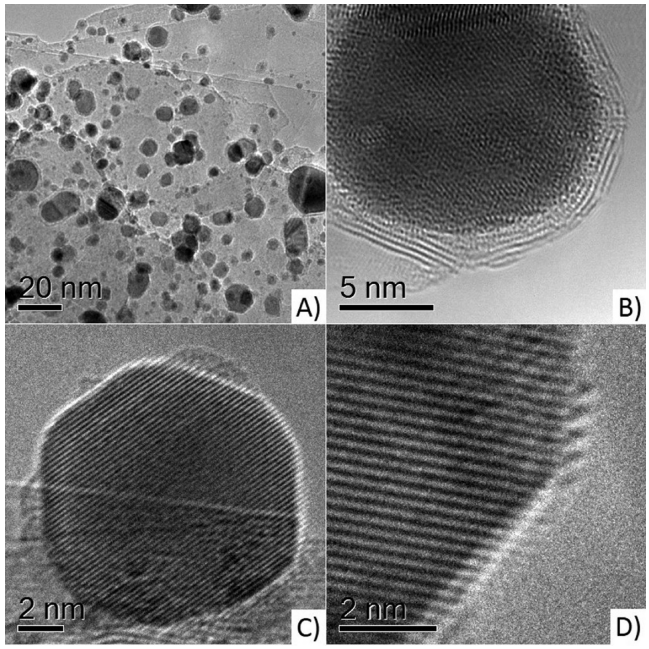

Figure 6. Ruthenium nanoparticles supported on boron nitride. In vacuum (A, B), all particles are encapsulated in boron nitride layers. Ruthenium nanoparticles supported on boron nitride in 3:1 H_2/N_2 at 450 °C, in which (C, D) the surfaces are exposed to the gas phase. Reproduced with permission from ref 68. Copyright 2001 American Association for the Advancement of Science.

environment consisting of a 3:1 mixture of H_2 and N_2 in the ETEM at a total pressure of about 500 Pa at ca. 550 °C, the surface layer was removed exposing the surface of the metal particles (see Figure 6C,D). A similar surface coverage was observed by Kowalczyk and co-workers for ruthenium supported on carbon.[73] After treatment in H_2/N_2, the surfaces of the metal particles revealed a periodic structure (see Figure 6D), which by electron energy-loss spectroscopy was shown to contain barium. As the promoter phase was observed on the surface of the active metal particles, the promotional effect was believed to be of electronic nature. This was, however, contested by other studies.[74,75]

dx.doi.org/10.1021/cs401148d | ACS Catal. 2014, 4, 1673−1685

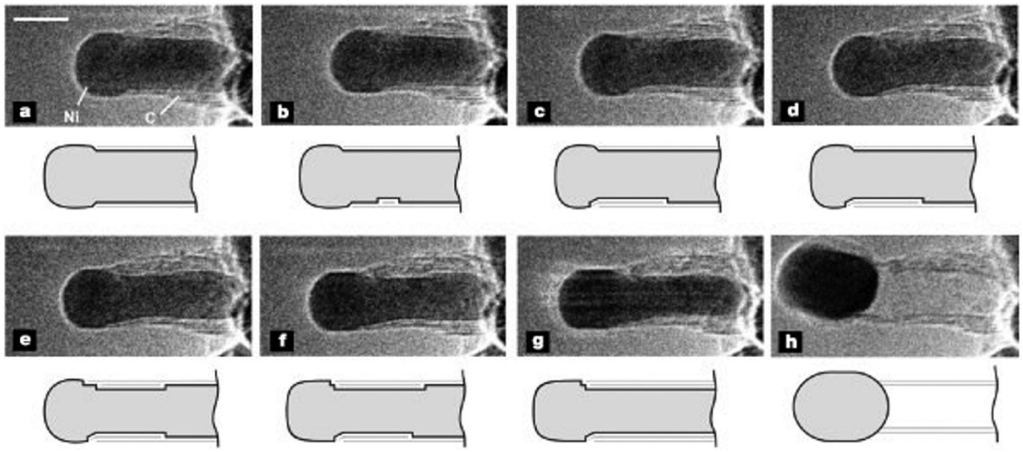

Figure 7. Image sequence of a growing carbon nanofiber illustrating an elongation/contraction process. Monoatomic Ni steps are found to be the point of formation for the carbon layers (guide-to-the-eye drawings are included in the figure). The images are acquired in situ with CH_4/H_2 = 1:1 at 210 Pa with the sample heated to 536 °C. Reproduced with permission from ref 78. Copyright 2004 Nature Publishing Group.

The striking difference in surface structure from vacuum to a reactive environment shows the significance of imaging catalytic metal nanoparticles under conditions resembling the operating environment if the true nature of the active site is to be unraveled.

CATALYST DEACTIVATION

Dynamic Studies – Growth and Oxidation of Carbon Structures. Catalyzed growth of extended carbon nanofiber structures in the form of either filaments or tubes have been a major point of interest. For instance, in nickel-based steam-reforming catalysts, the growth of carbon nanofibers resulting from low H_2O/C ratio or high temperature can have catastrophic effects.[76] When fibers grow inside catalyst pellets, they can break up the pellet structuring, leaving granulates blocking the reactor resulting in a high pressure drop.[77]

Helveg et al. studied the formation of fibrous carbon structures in a nickel-based steam reforming catalyst using environmental TEM.[78] In a 1:1 mixture of hydrogen and methane, growth of both carbon filaments or whiskers and carbon nanotubes (CNTs) was observed. Figure 7 illustrates the dynamically behavior of the Ni catalysts during CNT growth. On the basis of the experimental observation of the growth process and modeling by density functional theory (DFT), the authors concluded that that individual graphene layers of the carbon filaments were formed at step edges as the carbon atoms bind more strongly here. Details on the experiment are described by Helveg et al.[78] and the corresponding supplementary movies showing the growth.

In a related study, Koh et al. studied the oxidation of carbon nanotubes under an oxygen atmosphere at temperatures ranging from 300 to 520 °C.[79] Their observations indicated that the oxidation of CNTs is initiated at the side walls rather than the caps and proceeds layer by layer.

With stricter demands on emission control being enforced worldwide, oxidation of particulate matter from particularly diesel engines is a topic of increasing interest.[80] Simonsen et al. studied the oxidation of soot over a ceria catalyst[81] for vehicle emission control with emphasis on the soot–ceria interface under oxidizing conditions. As model soot, 30 nm carbon black particles were used. The study concluded that the oxidation occurs solely at the soot–ceria interface. A motion of the particles toward the interface, which established a continuous interface and an efficient reaction point, accompanied the oxidation of soot.

Sintering of Supported Metal Catalysts. Sintering or growth of nanoparticles is a deactivation route that plagues supported metal catalysis.[82] The phenomenon has been studied at great length using TEM under a controlled atmosphere from the time the technique became available.[17] More recent studies include both model systems,[45,46,83] as well as technical catalysts.[84–86]

Two mechanisms of mass transfer are suggested to be responsible for sintering of metal nanoparticles. One mechanism suggests that atomic species or small entities can migrate from smaller to larger particles due to a difference in chemical potential this is known as Ostwald ripening (OR). The other mechanism is particle migration and coalescence (PMC) where particles migrate on the substrate and coalesce into single particles as they encounter each other. Both mechanisms play a role in industrial catalysis, the dominant mechanism being determined by the reaction conditions. Traditionally, the shape of the particle size distribution after a given time on stream has been used to determine the mechanism of sintering. A tail on the small diameter side of the mean size indicated an OR mechanism, whereas a tail on the large diameter side of the mean indicates growth by PMC.[87,88]

Figure 8 shows images and size distributions of spinel-supported nickel nanoparticles determined from TEM images. First, the sample was reduced in 300 Pa H_2 at 500 °C (Figure 8a) and then exposed to the sintering environment, 200 Pa H_2 at 750 °C (Figure 8b) and 200 Pa H_2 and 200 Pa H_2O at 750 °C (Figure 8c) for 5 h. The particle size distributions after reduction and after sintering determined from a set of TEM images are shown in Figure 8d. Both distributions after sintering show a tail on the large diameter side of the mean, indicating that the growth occurred via PMC and a strong effect of atmosphere composition is observed. In order to further document the sintering mechanism, the particles were imaged during exposure to the sintering environments.[85] Based on these observations along with an observation of the initial exposure to a reactive environment,[89,90] Hansen et al. suggested that the sintering of supported metal nanoparticles could be divided into three phases.[85] In phase 1, a rapid decrease of activity is observed, and sintering is dominated by OR. During

dx.doi.org/10.1021/cs401148d | ACS Catal. 2014, 4, 1673–1685

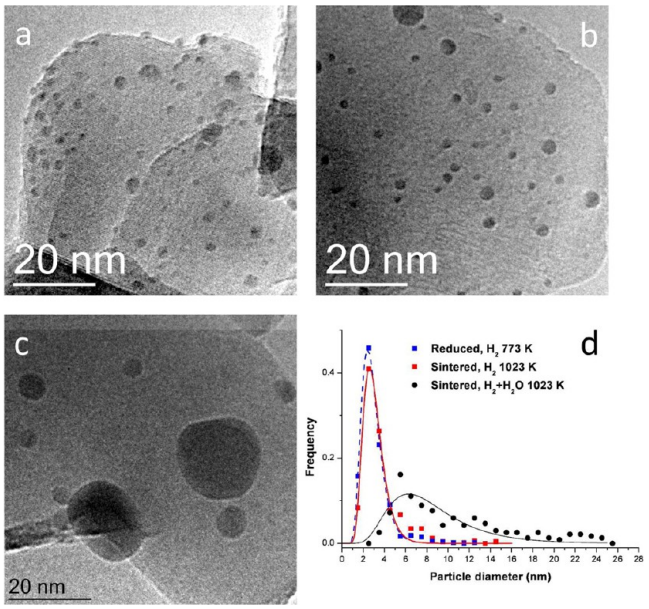

Figure 8. TEM images of a $Ni/MgAl_2O_4$ sample: (a) after reduction in 300 Pa H_2 at 500 °C; (b) after sintering for 5 h in 200 Pa H_2 at 750 °C; (c) after sintering for 5 h in 200 Pa H_2 and 200 Pa H_2O at 750 °C; (d) particle size distributions for the three cases. Reproduced with permission from ref 85. Copyright 2013 American Chemical Society.

this stage, the catalyst reaches its operating temperature and the metal particles attain their equilibrium shape. In phase 2, sintering slows down, but particles still grow in size, mainly via particle migration. Phase 3 represents the stable operation of the catalyst; the active particles have reached a size where migration is very slow.

SPECTROSCOPY AND CHEMICAL STATE

The ETEM not only provides images in direct space but also, with the necessary add-ons, the microscope will provide information about the chemical composition and chemical state of the constituent atoms of a catalyst. Electron-based spectroscopy in a TEM is an excellent tool for probing the composition or chemical state of a given sample at the local scale from the micrometer scale down to the atomic level.[91−95] The natural step when studying catalysts in a controlled atmosphere in the ETEM is to link the local chemical information to the structural evolution of the sample during gas treatment inside the microscope.

Although energy dispersive X-ray spectroscopy (EDX) is extensively used in the electron microscopy community for elemental composition analysis, there are technical difficulties using this technique in environmental TEM especially at elevated temperature, as the thermal radiation from heating holders saturates the EDX detector. Electron energy-loss spectroscopy (EELS) does not suffer from this limitation as the spectrometer measures the energy distribution of the primary electrons after interaction with the specimen. EELS has been used in several studies to probe the composition of a sample during in situ treatment in the ETEM. Chee and Sharma used core-loss EELS in order to follow the decomposition of carbon-containing iron precursors during heating.[96] Even though the study was performed under high-vacuum conditions, it showed the potential of in situ EELS measurements. Formation of the active state of the catalyst by reduction of oxidized precursors is a textbook example of how in situ EELS can elucidate the development of catalyst material at a local scale. In order to study the dispersion of Co nanoparticles as they were formed in the Fischer−Tropsch catalyst, Dehghan et al. used in situ EELS to probe the state of promoted cobalt at elevated temperature in a flow of hydrogen.[97] The authors showed the strength of local spectroscopy, as they were able to distinguish between the oxygen signal in the supporting alumina and the oxygen signal originating from oxidized cobalt nanoparticles. Another example of probing the development of catalyst particles is reported by Janbroers and co-workers.[98] They followed the

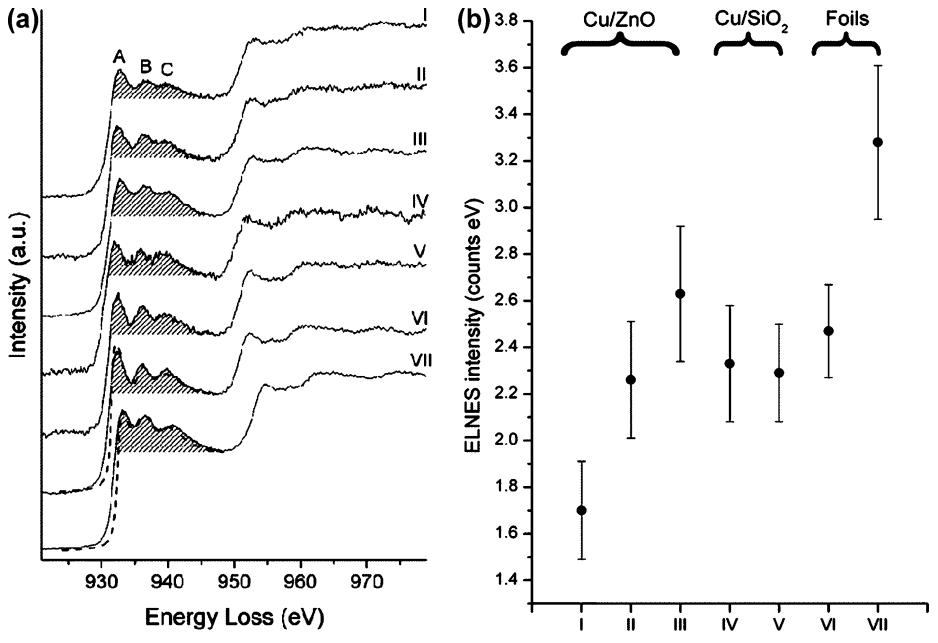

Figure 9. (a) In situ ELNES of the Cu $L_{2,3}$ edges. (b) Quantification of ELNES. Reproduced with permission from ref 53. Copyright 2003 American Chemical Society.

dx.doi.org/10.1021/cs401148d | ACS Catal. 2014, 4, 1673−1685

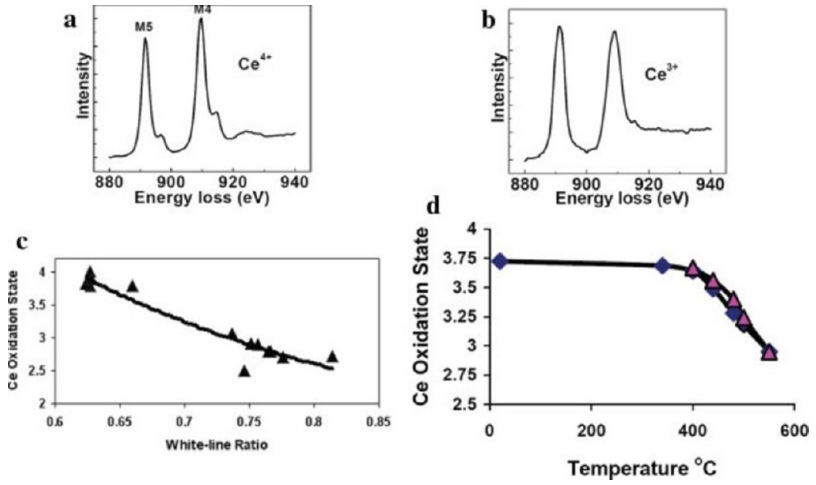

Figure 10. Background-subtracted electron energy-loss spectra showing Ce $M_{4,5}$ peaks (white-lines) at (a) room temperature and (b) at 685 °C. (c) Relationship between Ce oxidation state and white-line ratio. (d) Change in Ce oxidation state upon heating (squares) and cooling (triangles). Reproduced with permission from ref 112. Copyright 2009 Wiley.

reduction of iron oxide in an iron-based Fischer−Tropsch catalyst under CO treatment. Besides the reduction of the iron, the formation of an iron carbide was proven by means of in situ EELS and TEM at elevated temperature (270−400 °C).

One of the advantages of performing TEM-based EELS is the possibility to probe local inhomogeneity's in the composition of the material. Li et al. used EELS operating the TEM in STEM mode to yield a higher spatial resolution of the spectra.[99] However, the signal-to-noise ratio of the acquired spectra is diminished due to restrictions in the beam current density, which has to be relatively low to minimize electron-beam-related artifacts. By balancing the electron current density to give enough signal while minimizing the beam damage, it was possible to show a Ni enrichment at the surface of Ni−Cu bimetallics formed in situ in the TEM by means of EELS at 300 °C in a flow of H_2. Similarly the use of in situ analysis was carried out by the same authors to map the Ru promoter in a Co based Fischer−Tropsch catalyst.[100]

In addition to the quantitative compositional information retrieved from the EELS data, the fine structure of energy-loss near-edge structure (ELNES) of the spectra contains chemical state information about the elements.[101,102] As EELS probes the density of unoccupied states, the fine structure of the energy-loss edges is very sensitive to the chemical environment of the probed atom.[94]

Transition metals such as Fe, Ni, and Co, which in general are of great interest in catalysis, have characteristic peak-like features at their ionization edges known as *white-lines*. However, the 3d transition metal Cu has a more edge-like fine structure at the $L_{2,3}$ ionization edge due to a filled 3d band.[93] Probing an oxidized state of copper reveals white-lines in the Cu spectrum, as the d-band is no longer fully occupied. This drastic change in the fine structure of Cu $L_{2,3}$ ionization provides an easy way to follow the oxidation state of Cu.[33,103,104]

Wagner et al. showed that the fine structure of the metallic Cu L_3 ionization edge can be used to probe the alloying of Cu nanoparticles and Zn in a Cu/ZnO-based catalyst for methanol synthesis.[105] The fine structure of the edge was quantified and revealed alloy formation in the presence of CO in the surrounding atmosphere; whereas the reduction potential of pure H_2 is insufficient to surface reduce the ZnO necessary for creating the Cu−Zn alloy nanoparticles. The findings were backed up by a theoretical calculation of the EELS fine structure by the FEFF simulation software.[106] In Figure 9, the fine structure of the Cu L_3 edge has been quantified and compared to theoretical simulations in order to study the effect of strain and alloy formation. The morphology of the nanoparticles also plays an important role when drawing conclusions from EELS data.

In the case of nickel reduction, Jeangros et al. used the fine structure of the Ni $L_{2,3}$ ionization edges to quantify the reduction of NiO to Ni.[107] By following the degree of reduction in situ at different heating rates, the authors were able to calculate the activation energy of NiO reduction, showing the capability of quantitative in situ EELS. Another example of quantitative in situ EELS is the study of the redox behavior of cerium-based oxides,[108−111] where the authors have observed higher redox activity for structures with disordered cations. Figure 10 shows the dependency of the white-line ratio of Ce $M_{4,5}$ ionization edges on the oxidation state, which is studied as a function of temperature under reducing conditions.

Even though the work of Raabe et al. on the active state of manganese oxide compounds is not strictly speaking in situ EELS, the spectra are acquired in the ETEM in high vacuum after in situ treatment by H_2O without the sample leaving the microscope. Combined with imaging and crystallographic data, a good insight into the coupling of the valence state of the catalyst and the O_2 evolution from H_2O is obtained.[113]

Overall, in situ EELS proves to be an excellent way of probing the chemical state of materials during exposure to controlled gas atmosphere at elevated temperature. However, a relatively high electron beam dose is often used when focusing the electron beam for doing local probing of the chemical state by EELS. This increased electron dose enhances the possibility of beam-induced artifacts. Su et al. showed electron-beam-induced reduction of V_2O_5 and MoO_3 in vacuum using a conventional high-vacuum TEM.[114−116] Having gas species near the sample might increase similar effects, as the electron beam will ionize a part of the gas and change the reactivity of the gas species. Cavalca et al. reported that Cu_2O can be reduced to metallic copper in a H_2O environment by the electron beam. The Cu_2O sample did not change under similar electron irradiation conditions in vacuum.[103,104] Furthermore, the ionization of gas species will result in an increased

dx.doi.org/10.1021/cs401148d | *ACS Catal.* 2014, 4, 1673−1685

background of the electron energy-loss spectra, which has to be accounted for by, for instance, acquiring reference spectra of the gas alone. Addressing these issues is of the utmost importance in order to maintain the reliability of the EELS measurements during gas exposure.

In Situ EELS for Gas Detection and Quantification. It is obviously not only the solid state in the sample area of the microscope which gives rise to a signal in the electron energy-loss spectra. The ionization of the gas species results in characteristic features, both in the low-loss region of the spectra and at core-loss energies.[31,42,79,117] The energy-loss signal can be used quantitatively to measure the composition of the gas mixture admitted into the microscope when performing in situ experiments in much the same way as would be done with solids. However, as the gas occupies the volume between the pressure-limiting apertures, the scattering geometry is less well-defined and care has to be taken when setting up the microscope for such experiments.[117,118]

Using the low-loss region of the electron energy-loss spectrum for gas composition analysis allows for quantification of H_2 as well.[118] Quantitative gas composition analysis requires characteristic reference spectra from the individual gases used for multicomponent fitting. These spectra must be acquired at the same optical conditions in the microscope as used during an experiment. The low-loss method for gas composition requires that the electron beam only excites gas molecules and does not interact with the solid material. The signal from the solid will complicate the analysis as the spectral structure in the low-loss region is extremely sensitive to the chemical state of the solid and the signal strength is typically comparable to the signal from the gas phase.

Recently EELS has been used to address one of the major challenges in environmental TEM, especially in the field of catalysis: Is the sample in the TEM active in converting the reactants under the conditions used in the ETEM? Chenna and Crozier have shown that the EELS signal is a useful tool for in situ probing the conversion of CO to CO_2 over a Ru-based catalyst inside the microscope.[119] In order to increase the EELS signal, the authors developed a method to create a TEM sample with sufficiently high catalytic loading by impregnating 200 nm SiO_2 spheres with Ru and dispersing the resulting Ru/SiO_2 onto glass wool. The oxidation of CO to CO_2 as a function of temperature measured by means of in situ EELS is shown in Figure 11. The conversion is quantified by fitting a linear combination of CO and CO_2 reference spectra, showing the same trend for the catalytic reaction measured in situ in the microscope compared to catalytic tests performed in a dedicated reactor.[119]

Reference experiments without the catalyst using the hot stage and sample support alone have been conducted in order to ensure that the measured catalytic activity is solely due to the sample.

Even though EELS provides insight into the gas composition, spectroscopy and imaging have to be carried out serially. However, the switching time between spectroscopy mode and imaging mode is a matter of seconds/mins. The positive identification of a catalytic process taking place in the microscope by means of EELS is a step in the direction toward simultaneous catalytic activity measurement and microscopy, but the method is so far restricted to a limited number of gases.

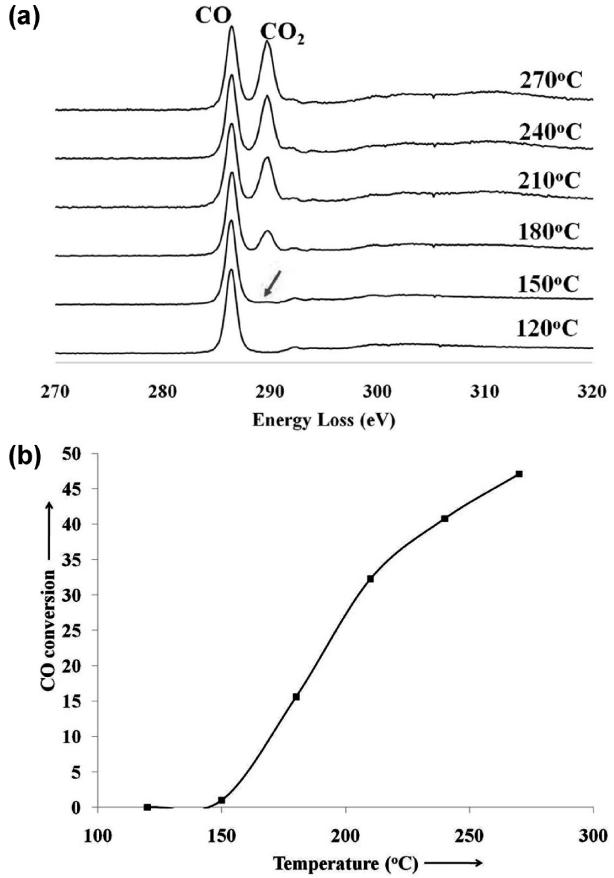

Figure 11. In situ EELS for probing gas conversion: (a) Background-subtracted energy-loss spectra acquired in situ at different temperatures during CO oxidation from a Ru/SiO_2 catalyst. (b) CO conversion versus temperature from a Ru/SiO_2 catalyst measured from in situ EELS. Reproduced from ref 119. Copyright 2012 American Chemical Society.

RECENT DEVELOPMENTS AND PROSPECTS

Recent developments within controlled atmosphere TEM have mainly revolved around limiting the drift while heating samples in dedicated heating holders and increasing the pressure limit of in situ experimentation. Interestingly enough, the approach to solving both these challenges has been the same: the application of microelectro−mechanical systems (MEMS).

One of the major reasons for sample drift during heating has been the bulkiness of conventional furnace-type heating holders. In such holders, a heating filament is encased in a ceramic and placed in a metal furnace with a thermocouple welded to it. This means that both the thermally insulating suspension of the furnace as well as the furnace itself will expand and contract in response to heating and cooling resulting in sample drift, typically several tens of micrometers. In order to minimize thermal drift, MEMS-based heaters are often used. These come in mainly two designs, either a miniaturized heating filament encapsulated in a thin membrane,[36,120−122] or an electron transparent electrically conductive film, which will heat resistively as current is passed through it.[123]

In order to image materials under higher pressure than what conventional differentially pumped ETEM can provide, a modified holder design incorporating electron transparent thin windows has been developed in parallel by Creemer et

dx.doi.org/10.1021/cs401148d | ACS Catal. 2014, 4, 1673−1685

al.[36] and de Jonge et al.,[37,124] similar to the design shown in Figure 12. Using this design, Alan et al. was able to show

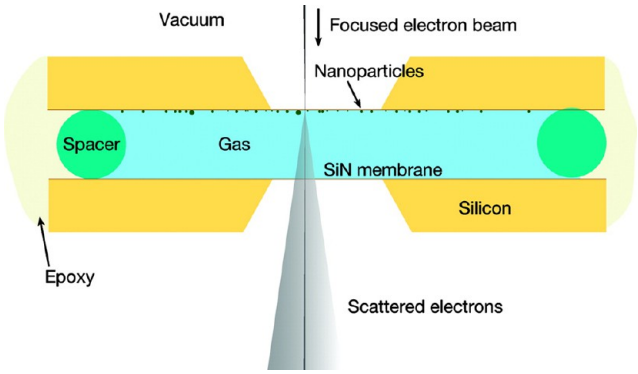

Figure 12. Schematic of closed cell TEM holder for atmospheric pressure scanning transmission electron microscopy (STEM). A sample compartment filled with gas at atmospheric pressure is enclosed between two silicon microchips supporting electron-transparent SiN windows separated by a spacer. The dimensions and angles are not to scale. Reproduced with permission from ref 37. Copyright 2010 American Chemical Society.

hydrogenation of palladium particles at 400 kPa pressure at 240 °C,[125,126] as verified by electron diffraction. Similarly, dehydrogenation was observed under the same pressure when the temperature was decreased to room temperature. Creemer et al. have demonstrated imaging of growing copper nanoparticles under 120 kPa at temperatures up to 500 °C.[122] Using carbon-based windows, Kawasaki et al. have designed a cell with windows thinner than 10 nm, resulting in less disturbance of the imaging properties of the microscope, and they have sustainably exposed a Au/TiO_2 sample to 1% CO in air at 1200 Pa.[127]

Vendelbo et al. used the combination of a TEM holder confining the gas by electron transparent SiN membranes and EELS to address another problematical issue when carrying out in situ electron microscopy: What is the temperature of the probed sample area?

The authors used the low-loss region of the energy-loss spectrum to estimate the local projected density of H_2 in the TEM holder at different temperatures keeping the pressure constant at 120 Pa. Figure 13 shows the effect on the EELS signal at elevated temperatures. The normalized ratio of inelastically scattered electrons gives the density of the probed hydrogen molecules. Calibrating the measured local H_2 density to a global density and temperature via the ideal gas law, the local temperature is estimated.[128] The additional signal from the SiN-confining membranes was taken into account by subtracting the signal from an empty cell. Using this method, the authors were able to estimate the temperature gradient over the heating device to be on the order of 50 °C at 500 °C. Further information on the detailed data analysis is given by Vendelbo et al.[128]

In order to minimize the effects of the electron beam on the sample, as few as possible electrons must interact with the sample. This in effect means that we have to make the most out of each electron. Recently, new developments within the area of more efficient and faster electron detection have been made. Using direct electron detection cameras, the need for the fluorescent coating used in conventional CCD cameras can be omitted, resulting in a higher electron collection efficiency.

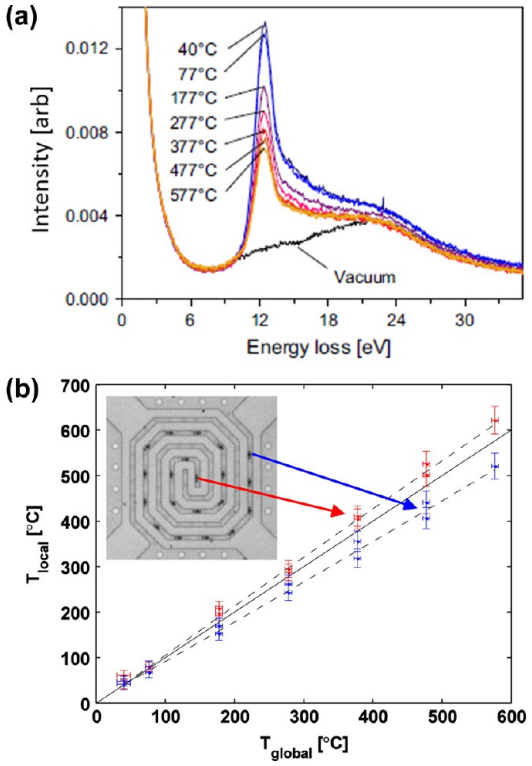

Figure 13. Probing the local temperature by EELS. (a) Electron energy-loss spectra of the nanoreactor at 120 Pa H_2 at different temperatures in the interval T = 40−577 °C. The feature at 12.4 eV is attributed to the hydrogen ionization edge. (b) Local temperature (T_{local}) based on EELS measurements at the center (red, upper data points) and edge (blue, lower data points) windows as a function of the global temperature (T_{global}) from resistivity measurements. Reproduced with permission from ref 128. Copyright 2013 Elsevier.

Furthermore, high-speed computers facilitate faster read out and signal processing, resulting in lower dead time of the cameras.[129] This does not only enable us to limit the electron dose to which samples are exposed but also allows us to image transient phenomena with millisecond resolution.

Recent development in four-dimensional ultrafast electron microscopy (4D UEM) gives the possibility for imaging processes in the femtosecond regime.[130] The basic idea behind these highly specialized TEMs is the synchronization of an electron pulse used for imaging and a stimulus of the sample (e.g., heating). This way, high temporal resolution of irreversible reactions can be obtained. In order to have enough electrons in the electron pulse, to image the sample the density of electrons is so high that Coulomb repulsion is limiting the coherence of the electron beam. That results in a somewhat lower spatial resolution than can be obtained in more traditional TEMs. However, 4D UEM shows great potential for imaging at the time scale of chemical reactions.

The effect of the electron beam is only one of the effects that can misguide the operator to noncritically transfer local observations to the global scheme. Electron microscopy in general and ETEM in particular relies considerably on complementary techniques in order to ensure that local effects probed by TEM are representative for the sample as a whole. As an example, the combination of ETEM and in situ EXAFS has been used for studying the morphology of Cu nanoparticles.[2,52] However, the studies are performed in separate experimental setups. Bringing more characterization techniques

dx.doi.org/10.1021/cs401148d | ACS Catal. 2014, 4, 1673−1685

together in one instrument might be, despite the increased complexity, a beneficial addendum to the ETEM community. As an example, several groups bring light into the microscope via special TEM sample holders, facilitating light input by fiber optics, or add the light source directly to the microscope column.[104,131] Light can be guided out of the microscope in the same way. Cathodoluminescence is already possible with dedicated equipment in the microscope, but to the authors' knowledge, it has not been reported used in combination with a gaseous environment. Having the light-in and the light-out capabilities, it is straightforward to imagine the combination of electron spectroscopy and optical spectroscopy such as Raman spectroscopy and Plasmon resonance spectroscopy in environmental TEM by optimizing the collection solid angle of the optical response signal.

CONCLUSIONS

The investigation of catalysts in a reactive environment can be a daunting feat scientifically as well as technically. Catalysts are dynamic entities and their state and structure changes with their surroundings and over time. Environmental transmission electron microscopy provides a tool for imaging samples at the atomic scale with simultaneous acquisition of spectroscopic information, all in a simulated working environment. Having this tool in the toolbox provides information on the local level that can ultimately dictate the development of the next generation of catalysts and functional materials when combined with other more globally probing characterization and analysis tools.

AUTHOR INFORMATION

Corresponding Author

*E-mail: twh@cen.dtu.dk.

Notes

The authors declare no competing financial interest.

REFERENCES

(1) Chorkendorff, I.; Niemantsverdriet, J. W. *Concepts of Modern Catalysis and Kinetics*; Wiley-VCH: Weinheim, 2003.
(2) Grunwaldt, J. D.; Molenbroek, A. M.; Topsoe, N. Y.; Topsoe, H.; Clausen, B. S. *J. Catal.* **2000**, *194*, 452−460.
(3) Honkala, K.; Hellman, A.; Remediakis, I. N.; Logadottir, A.; Carlsson, A.; Dahl, S.; Christensen, C. H.; Norskov, J. K. *Science* **2005**, *307*, 555−558.
(4) Brodersen, S. H.; Gronbjerg, U.; Hvolbaek, B.; Schiotz, J. *J. Catal.* **2011**, *284*, 34−41.
(5) Boudart, M. *Chem. Rev.* **1995**, *95*, 661−666.
(6) Datye, A. K. *J. Catal.* **2003**, *216*, 144−154.
(7) Hansen, P. L.; Helveg, S.; Datye, A. K., Atomic-scale imaging of supported metal nanocluster catalysts in the working state. In *Adv. Catal.*; Gates, B. C., Knoziner, H., Eds.; Academic Press, London, U.K., 2006; Vol. *50*, pp 77−95.
(8) Zhang, S. R.; Nguyen, L.; Zhu, Y.; Zhan, S. H.; Tsung, C. K.; Tao, F. *Acc. Chem. Res.* **2013**, *46*, 1731−1739.
(9) Gai, P. L.; Boyes, E. D.; Helveg, S.; Hansen, P. L.; Giorgio, S.; Henry, C. R. *MRS Bull.* **2007**, *32*, 1044−1050.
(10) Grunwaldt, J. D.; Wagner, J. B.; Dunin-Borkowski, R. E. *ChemCatChem.* **2013**, *5*, 62−80.
(11) Ruska, E. *Kolloid-Z.* **1942**, *100*, 212−219.
(12) Swann, P. R.; Tighe, N. J. *JKA-Jernkontoret Ann.* **1971**, *155*, 497.
(13) Hashimoto, H.; Naiki, T. *Jpn. J. Appl. Phys.* **1968**, *7*, 946−952.
(14) Baker, R. T. K.; Harris, P. S. *J. Phys. E: Sci. Instrum.* **1972**, *5*, 793.
(15) Boyes, E. D.; Gai, P. L. *Ultramicroscopy* **1997**, *67*, 219−232.
(16) Baker, R. T. K.; Barber, M. A.; Harris, P. S.; Feates, F. S.; Waite, R. J. *J. Catal.* **1972**, *26*, 51−62.
(17) Baker, R. T. K.; Harris, P. S.; Thomas, R. B. *Surf. Sci.* **1974**, *46*, 311−316.
(18) Ross, F. M.; Tersoff, J.; Reuter, M.; Legoues, F. K.; Tromp, R. M. *Microsc. Res. Tech.* **1998**, *42*, 281−294.
(19) Gai, P. L.; Kourtakis, K. *Science* **1995**, *267*, 661−663.
(20) Gai, P. L. *Curr. Opin. Solid State Mater. Sci.* **1999**, *4*, 63−73.
(21) He, M.; Jiang, H.; Liu, B.; Fedotov, P. V.; Chernov, A. I.; Obraztsova, E. D.; Cavalca, F.; Wagner, J. B.; Hansen, T. W.; Anoshkin, I. V.; Obraztsova, E. A.; Belkin, A. V.; Sairanen, E.; Nasibulin, A. G.; Lehtonen, J.; Kauppinen, E. I. *Sci. Rep.* **2013**, *3*, 1460.
(22) Sharma, R.; Iqbal, Z. *Appl. Phys. Lett.* **2004**, *84*, 990−992.
(23) Hofmann, S.; Sharma, R.; Ducati, C.; Du, G.; Mattevi, C.; Cepek, C.; Cantoro, M.; Pisana, S.; Parvez, A.; Cervantes-Sodi, F.; Ferrari, A. C.; Dunin-Borkowski, R.; Lizzit, S.; Petaccia, L.; Goldoni, A.; Robertson, J. *Nano Lett.* **2007**, *7*, 602−608.
(24) Yoshida, H.; Kohno, H.; Takeda, S. *Micron* **2012**, *43*, 1176−1180.
(25) Feng, X. F.; Chee, S. W.; Sharma, R.; Liu, K.; Xie, X.; Li, Q. Q.; Fan, S. S.; Jiang, K. L. *Nano Res.* **2011**, *4*, 767−779.
(26) Yoshida, H.; Takeda, S.; Uchiyama, T.; Kohno, H.; Homma, Y. *Nano Lett.* **2008**, *8*, 2082−2086.
(27) Pattinson, S. W.; Diaz, R. E.; Stelmashenko, N. A.; Windle, A. H.; Ducati, C.; Stach, E. A.; Koziol, K. K. K. *Chem. Mater.* **2013**, *25*, 2921−2923.
(28) van Dorp, W. F.; Lazic, I.; Beyer, A.; Goelzhaeuser, A.; Wagner, J. B.; Hansen, T. W.; Hagen, C. W. *Nanotechnology* **2011**, *22*, 115303.
(29) Booth, T. J.; Pizzocchero, F.; Andersen, H.; Hansen, T. W.; Wagner, J. B.; Jinschek, J. R.; Dunin-Borkowski, R. E.; Hansen, O.; Boggild, P. *Nano Lett.* **2011**, *11*, 2689−2692.
(30) Boyes, E. D.; Ward, M. R.; Lari, L.; Gai, P. L. *Ann. Phys.* **2013**, *525*, 423−429.
(31) Hansen, T. W.; Wagner, J. B.; Dunin-Borkowski, R. E. *Mater. Sci. Technol.* **2010**, *26*, 1338−1344.
(32) Kishita, K.; Sakai, H.; Tanaka, H.; Saka, H.; Kuroda, K.; Sakamoto, M.; Watabe, A.; Kamino, T. *J. Electron. Microsc.* **2009**, *58*, 331−339.
(33) Tanaka, N.; Usukura, J.; Kusunoki, M.; Saito, Y.; Sasaki, K.; Tanji, T.; Muto, S.; Arai, S. *Microscopy* **2013**, *62*, 205−215.
(34) Sharma, R. *Microsc. Microanal.* **2001**, *7*, 494−506.
(35) Takeda, S.; Yoshida, H. *Microscopy* **2013**, *62*, 193−203.
(36) Creemer, J. F.; Helveg, S.; Hoveling, G. H.; Ullmann, S.; Molenbroek, A. M.; Sarro, P. M.; Zandbergen, H. W. *Ultramicroscopy* **2008**, *108*, 993−998.
(37) de Jonge, N.; Bigelow, W. C.; Veith, G. M. *Nano Lett.* **2010**, *10*, 1028−1031.
(38) Hansen, T. W.; Wagner, J. B. *Microsc. Microanal.* **2012**, *18*, 684−690.
(39) Yoshida, H.; Takeda, S. *Phys. Rev. B* **2005**, *72*, 195428.
(40) Suzuki, M.; Yaguchi, T.; Zhang, X. F. *Microscopy* **2013**, *62*, 437−450.
(41) Wagner, J. B.; Cavalca, F.; Damsgaard, C. D.; Duchstein, L. D. L.; Hansen, T. W. *Micron* **2012**, *43*, 1169−1175.
(42) Jinschek, J. R.; Helveg, S. *Micron* **2012**, *43*, 1156−1168.
(43) Haider, M.; Rose, H.; Uhlemann, S.; Schwan, E.; Kabius, B.; Urban, K. *Ultramicroscopy* **1998**, *75*, 53−60.
(44) Freitag, B.; Kujawa, S.; Mul, P. M.; Ringnalda, J.; Tiemeijer, P. C. *Ultramicroscopy* **2005**, *102*, 209−214.
(45) Simonsen, S. B.; Chorkendorff, I.; Dahl, S.; Skoglundh, M.; Sehested, J.; Helveg, S. *J. Am. Chem. Soc.* **2010**, *132*, 7968−7975.
(46) Simonsen, S. B.; Chorkendorff, I.; Dahl, S.; Skoglundh, M.; Sehested, J.; Helveg, S. *J. Catal.* **2011**, *281*, 147−155.
(47) Kuwauchi, Y.; Yoshida, H.; Akita, T.; Haruta, M.; Takeda, S. *Angew. Chem., Int. Ed.* **2012**, *51*, 7729−7733.
(48) Gryaznov, V. G.; Kaprelov, A. M.; Belov, A. Y. *Philos. Mag. Lett.* **1991**, *63*, 275−279.
(49) Howe, J. M.; Yokota, T.; Murayama, M.; Jesser, W. A. *J. Electron. Microsc.* **2004**, *53*, 107−114.
(50) Doraiswamy, N.; Marks, L. D. *Surf. Sci.* **1996**, *348*, L67−L69.

(51) Yoshida, H.; Kuwauchi, Y.; Jinschek, J. R.; Sun, K. J.; Tanaka, S.; Kohyama, M.; Shimada, S.; Haruta, M.; Takeda, S. *Science* **2012**, *335*, 317−319.
(52) Hansen, P. L.; Wagner, J. B.; Helveg, S.; Rostrup-Nielsen, J. R.; Clausen, B. S.; Topsøe, H. *Science* **2002**, *295*, 2053−2055.
(53) Wagner, J. B.; Hansen, P. L.; Molenbroek, A. M.; Topsøe, H.; Clausen, B. S.; Helveg, S. *J. Phys. Chem. B* **2003**, *107*, 7753−7758.
(54) Topsoe, N. Y.; Topsoe, H. *J. Mol. Catal. A* **1999**, *141*, 95−105.
(55) Askgaard, T. S.; Norskov, J. K.; Ovesen, C. V.; Stoltze, P. *J. Catal.* **1995**, *156*, 229−242.
(56) Wagner, J. B. In situ transmission electron microscopy of catalyst particles. Ph.D. Thesis, University of Copenhagen, November 2002.
(57) Cabie, M.; Giorgio, S.; Henry, C. R.; Axet, M. R.; Philippot, K.; Chaudret, B. *J. Phys. Chem. C* **2010**, *114*, 2160−2163.
(58) Giorgio, S.; Cabie, M.; Henry, C. R. *Gold Bull.* **2008**, *41*, 167−173.
(59) Molina, L. M.; Lee, S.; Sell, K.; Barcaro, G.; Fortunelli, A.; Lee, B.; Seifert, S.; Winans, R. E.; Elam, J. W.; Pellin, M. J.; Barke, I.; von Oeynhausen, V.; Lei, Y.; Meyer, R. J.; Alonso, J. A.; Rodriguez, A. F.; Kleibert, A.; Giorgio, S.; Henry, C. R.; Meiwes-Broer, K. H.; Vajda, S. *Catal. Today* **2011**, *160*, 116−130.
(60) Hammer, B.; Nørskov, J. K. *Nature* **1995**, *376*, 238.
(61) Haruta, M.; Yamada, N.; Kobayashi, T.; Iijima, S. *J. Catal.* **1989**, *115*, 301−309.
(62) Haruta, M.; Tsubota, S.; Kobayashi, T.; Kageyama, H.; Genet, M. J.; Delmon, B. *J. Catal.* **1993**, *144*, 175−192.
(63) Akita, T.; Kohyama, M.; Haruta, M. *Acc. Chem. Res.* **2013**, *46*, 1773−1782.
(64) Akita, T.; Lu, P.; Ichikawa, S.; Tanaka, K.; Haruta, M. *Surf. Interface Anal.* **2001**, *31*, 73−78.
(65) Kresse, G.; Hafner, J. *Phys. Rev. B* **1993**, *48*, 13115−13118.
(66) Uchiyama, T.; Yoshida, H.; Kuwauchi, Y.; Ichikawa, S.; Shimada, S.; Haruta, M.; Takeda, S. *Angew. Chem., Int. Ed.* **2011**, *50*, 10157−10160.
(67) Jacobsen, C. J. H. *J. Catal.* **2001**, *200*, 1−3.
(68) Hansen, T. W.; Wagner, J. B.; Hansen, P. L.; Dahl, S.; Topsoe, H.; Jacobsen, C. J. H. *Science* **2001**, *294*, 1508−1510.
(69) Hansen, T. W.; Hansen, P. L.; Dahl, S.; Jacobsen, J. H. *Catal. Lett.* **2002**, *84*, 7−12.
(70) Kowalczyk, Z.; Jodzis, S.; Sentek, J. *Appl. Catal., A* **1996**, *138*, 83−91.
(71) Tauster, S. J.; Fung, S. C.; Garten, R. L. *J. Am. Chem. Soc.* **1978**, *100*, 170−175.
(72) Tauster, S. J. *Acc. Chem. Res.* **1987**, *20*, 389−394.
(73) Kowalczyk, Z.; Jodzis, S.; Raróg, W.; Zielínski, J.; Pielaszek, J.; Presz, A. *Appl. Catal., A* **1999**, *184*, 95−102.
(74) Szmigiel, D.; Zielinski, J.; Bielawa, H.; Kurtz, M.; Hinrichsen, O.; Muhler, M.; Rarog, W.; Jodzis, S.; Kowalczyk, Z.; Znak, L. *J. Catal.* **2002**, *205*, 205−212.
(75) Raróg, W.; Kowalczyk, Z.; Sentek, J.; Skladanowski, D.; Zielínski, J. *Catal. Lett.* **2000**, *68*, 163−168.
(76) Rostrup-Nielsen, J.; Christiansen, L. J. *Concepts in Syngas Manufacture*; Imperial College Press: London, U.K., 2011; Vol. *10*.
(77) Rostrup-Nielsen, J. R. *Steam Reforming Catalysts*. Danish Technical Press Inc.: 1975.
(78) Helveg, S.; Lopez-Cartes, C.; Sehested, J.; Hansen, P. L.; Clausen, B. S.; Rostrup-Nielsen, J. R.; Abild-Pedersen, F.; Nørskov, J. K. *Nature* **2004**, *427*, 426−429.
(79) Koh, A. L.; Gidcumb, E.; Zhou, O.; Sinclair, R. *ACS Nano* **2013**, *7*, 2566−2572.
(80) van Setten, B.; Makkee, M.; Moulijn, J. A. *Catal. Rev. Sci. Eng.* **2001**, *43*, 489−564.
(81) Simonsen, S. B.; Dahl, S.; Johnson, E.; Helveg, S. *J. Catal.* **2008**, *255*, 1−5.
(82) Sehested, J. *Catal. Today* **2006**, *111*, 103−110.
(83) Benavidez, A. D.; Kovarik, L.; Genc, A.; Agrawal, N.; Larsson, E. M.; Hansen, T. W.; Karim, A. M.; Datye, A. K. *ACS Catal.* **2012**, *2*, 2349−2356.
(84) Hansen, T. W. Sintering and particle dynamics in supported metal catalysts. Ph.D. Thesis, Technical University of Denmark: Lyngby, 2006.
(85) Hansen, T. W.; Delariva, A. T.; Challa, S. R.; Datye, A. K. *Acc. Chem. Res.* **2013**, *46*, 1720−1730.
(86) Liu, R. J.; Crozier, P. A.; Smith, C. M.; Hucul, D. A.; Blackson, J.; Salaita, G. *Microsc. Microanal.* **2004**, *10*, 77−85.
(87) Wynblatt, P.; Gjostein, N. A. *Prog. Solid State Chem.* **1975**, *9*, 21−58.
(88) Granqvist, C. G.; Buhrman, R. A. *Appl. Phys. Lett.* **1975**, *27*, 693−694.
(89) DeLaRiva, A. T.; Hansen, T. W.; Challa, S. R.; Datye, A. K. *J. Catal.* **2013**, *308*, 291−305.
(90) Challa, S. R.; Delariva, A. T.; Hansen, T. W.; Helveg, S.; Sehested, J.; Hansen, P. L.; Garzon, F.; Datye, A. K. *J. Am. Chem. Soc.* **2011**, *133*, 20672−20675.
(91) Friel, J. J.; Lyman, C. E. *Microsc. Microanal.* **2006**, *12*, 2−25.
(92) Watanabe, M. *Microscopy* **2013**, *62*, 217−41.
(93) Keast, V. J.; Scott, A. J.; Brydson, R.; Williams, D. B.; Bruley, J. *J. Microsc.* **2001**, *203*, 135−175.
(94) Egerton, R. F.; Malac, M. *J. Electron Spectrosc.* **2005**, *143*, 43−50.
(95) Egerton, R. F. *Rep. Prog. Phys.* **2009**, *72*, 016502.
(96) Chee, S. W.; Sharma, R. *Micron* **2012**, *43*, 1181−1187.
(97) Dehghan, R.; Hansen, T. W.; Wagner, J. B.; Holmen, A.; Rytter, E.; Borg, O.; Walmsley, J. C. *Catal. Lett.* **2011**, *141*, 754−761.
(98) Janbroers, S.; Crozier, P. A.; Zandbergen, H. W.; Kooyman, P. J. *Appl. Catal., B* **2011**, *102*, 521−527.
(99) Li, P.; Liu, J.; Nag, N.; Crozier, P. A. *J. Catal.* **2009**, *262*, 73−82.
(100) Li, P.; Liu, J.; Nag, N.; Crozier, P. *Appl. Catal., A* **2006**, *307*, 212−221.
(101) García de Abajo, F. J. *Rev. Mod. Phys.* **2010**, *82*, 209−275.
(102) Tan, H. Y.; Verbeeck, J.; Abakumov, A.; Van Tendeloo, G. *Ultramicroscopy* **2012**, *116*, 24−33.
(103) Cavalca, F.; Laursen, A. B.; Wagner, J. B.; Damsgaard, C. D.; Chorkendorff, I.; Hansen, T. W. *ChemCatChem.* **2013**, *5*, 2667−2672.
(104) Cavalca, F.; Laursen, A. B.; Kardynal, B. E.; Dunin-Borkowski, R. E.; Dahl, S.; Wagner, J. B.; Hansen, T. W. *Nanotechnology* **2012**, *23*, 075705.
(105) Wagner, J. B.; Hansen, P. L.; Molenbroek, A. M.; Topsoe, H.; Clausen, B. S.; Helveg, S. *J. Phys. Chem. B* **2003**, *107*, 7753−7758.
(106) Ankudinov, A. L.; Ravel, B.; Rehr, J. J.; Conradson, S. D. *Phys. Rev. B* **1998**, *58*, 7565−7576.
(107) Jeangros, Q.; Hansen, T. W.; Wagner, J. B.; Damsgaard, C. D.; Dunin-Borkowski, R. E.; Hebert, C.; Van Herle, J.; Hessler-Wyser, A. *J. Mater. Sci.* **2013**, *48*, 2893−2907.
(108) Wang, R.; Crozier, P. A.; Sharma, R.; Adams, J. B. *Nano Lett.* **2008**, *8*, 962−967.
(109) Sharma, R.; Crozier, P. A.; Kang, Z. C.; Eyring, L. *Philos. Mag.* **2004**, *84*, 2731−2747.
(110) Crozier, P. A.; Wang, R.; Sharma, R. *Ultramicroscopy* **2008**, *108*, 1432−40.
(111) Sharma, R. *Microsc. Res. Tech.* **2009**, *72*, 144−52.
(112) Sharma, R. *Microsc. Res. Tech.* **2009**, *72*, 144−152.
(113) Raabe, S.; Mierwaldt, D.; Ciston, J.; Uijttewaal, M.; Stein, H.; Hoffmann, J.; Zhu, Y.; Bloechl, P.; Jooss, C. *Adv. Funct. Mater.* **2012**, *22*, 3378−3388.
(114) Su, D. S. *Anal. Bioanal. Chem.* **2002**, *374*, 732−735.
(115) Su, D. S.; Wieske, M.; Beckmann, E.; Blume, A.; Mestl, G.; Schlogl, R. *Catal. Lett.* **2001**, *75*, 81−86.
(116) Wang, D.; Su, D. S.; Schlogl, R. *Z. Anorg. Allg. Chem.* **2004**, *630*, 1007−1014.
(117) Chenna, S.; Crozier, P. A. *Micron* **2012**, *43*, 1188−1194.
(118) Crozier, P. A.; Chenna, S. *Ultramicroscopy* **2011**, *111*, 177−85.
(119) Chenna, S.; Crozier, P. A. *ACS Catal.* **2012**, *2*, 2395−2402.
(120) Creemer, J. F.; Briand, D.; Zandbergen, H. W.; van der Vlist, W.; de Boer, C. R.; de Rooij, N. F.; Sarro, P. M. *Sens. Actuators, A* **2008**, *148*, 416−421.
(121) Creemer, J. F.; Van der Vlist, W.; Boer, C. R. D.; Zandbergen, H. W.; Sarro, P. M.; Briand, D.; De Rooij, N. F. *2005 Ieee Sensors*;

Institute of Electrical and Electronics Engineers: New York, 2005; Vols. *1* and *2*, pp 330−333.
(122) Creemer, J. F.; Helveg, S.; Kooyman, P. J.; Molenbroek, A. M.; Zandbergen, H. W.; Sarro, P. M. *J. Microelectromech. S.* **2010**, *19*, 254−264.
(123) Allard, L. F.; More, K. L.; Liu, J. *Microsc. Microanal.* **2009**, *15*, 130−131.
(124) de Jonge, N.; Peckys, D. B.; Kremers, G. J.; Piston, D. W. *Proc. Natl. Acad. Sci. U.S.A.* **2009**, *106*, 2159−2164.
(125) Alan, T.; Yokosawa, T.; Gaspar, J.; Pandraud, G.; Paul, O.; Creemer, F.; Sarro, P. M.; Zandbergen, H. W. *Appl. Phys. Lett.* **2012**, *100*, 081903.
(126) Yokosawa, T.; Alan, T.; Pandraud, G.; Dam, B.; Zandbergen, H. *Ultramicroscopy* **2012**, *112*, 47−52.
(127) Kawasaki, T.; Ueda, K.; Ichihashi, M.; Tanji, T. *Rev. Sci. Instrum.* **2009**, *80*, 5.
(128) Vendelbo, S. B.; Kooyman, P. J.; Creemer, J. F.; Morana, B.; Mele, L.; Dona, P.; Nelissen, B. J.; Helveg, S. *Ultramicroscopy* **2013**, *133*, 72−79.
(129) Grob, P.; Bean, D.; Typke, D.; Li, X. M.; Nogales, E.; Glaeser, R. M. *Ultramicroscopy* **2013**, *133*, 1−7.
(130) Flannigan, D. J.; Zewail, A. H. *Acc. Chem. Res.* **2012**, *45*, 1828−1839.
(131) Miller, B. K.; Crozier, P. A. *Microsc. Microanal.* **2013**, *19*, 461−469.